ACADEMIA ROMÂNĂ
Revue Roumaine de Chimie
https://www.icf.ro/rrch/

Rev. Roum. Chim.,
2023, *68*(7–8), 347–355
DOI: 10.33224/rrch.2023.68.7-8.04

Dedicated to Dr. Niculae I. Ionescu
on the occasion of his 90th anniversary

MORPHOLOGICAL PROPERTIES OF ZnO NANOSTRUCTURES DOPED WITH Ag AND Li FOR PIEZOELECTRIC APPLICATIONS

Mariana CHELU,[a,*] Mihai ANASTASESCU,[a] Jose CALDERON MORENO,[a] Daiana MITREA,[a] Hermine STROESCU,[a] Marin GHEORGHE[b] and Mariuca GARTNER [a]

[a]Roumanian Academy, "Ilie Murgulescu" Institute of Physical Chemistry, 202 Spl. Independentei, 060021 Bucharest, Roumania
[b]NANOM MEMS SRL, Rasnov, Roumania

Received November 30, 2022

The development of a facile method to obtain materials with piezoelectric properties, through a green synthesis, as an alternative to lead-free materials, was the main objective of this work. Piezo active materials were grown by chemical methods on two types of metal substrates: Pt/Ti/SiO_2/Si and the Ti foil. Ag and Li-doped ZnO nanostructures were prepared by hydrothermal method at low temperature on metallic substrates which were previously covered with ZnO seed layer deposited by spin coating sol-gel method. The newly prepared materials were covered with a polymer layer and were morphological characterized by atomic force microscopy (AFM) and scanning electron microscopy (SEM). The piezoelectric properties were estimated by measuring the direct piezoelectric coefficient d_{33}. The test results show that the doped ZnO nanostructures synthesized using a green route exhibit a piezoelectric response so the established method can be considered a promising approach for obtaining piezoelectric materials on large surfaces. Piezo active nanostructures could be of interest for integration into piezoelectric devices.

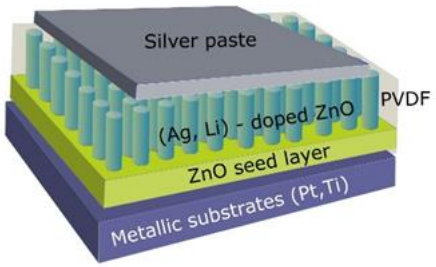

INTRODUCTION

Often mentioned to as *smart materials* or top models, piezoelectric materials can convert mechanical energy into electrical energy and vice versa.[1-3] The key to piezoelectric performance and functionality involves choosing and designing the suitable materials for a small-scale energy harvesting application.[4] Based on their direct piezoelectric effect, piezoelectric materials can be assembled to form diverse piezoelectric nanogenerators (NG).[5-7] When an external stress is applied, they are deformed, polarized charges are produced on the surface and an electrical response quickly results which can be harnessed.[8] NG are very attractive and are widely used in harvesting any form of mechanical energy from abundant and easily available sources in the environment, including human movements or activities, vibrations, air, water flow, etc.[9,10] Different piezoelectric NG have been manufactured based on nanostructured piezo active materials[11] such as: lead zirconate titanate (PZT), zinc oxide (ZnO), barium titanate ($BaTiO_3$), gallium nitride (GaN) and polyvinylidene fluoride (PVDF).[12-14] Among them, ZnO nanomaterials are biocompatible[15] and can be obtained in the form of high-quality crystals through accessible and environmentally friendly synthesis procedures, such as the sol-gel and hydrothermal

* Corresponding author: mchelu@icf.ro; mariana.chelu@gmail.com; tel.: +40-21-3121147

methods.[16-19] PVDF exhibit four distinct crystalline phases (alpha, beta, gamma and delta), of which only the beta phase shows important piezoelectric properties. However, the electroactive beta phase also requires polarization under certain conditions of temperature and voltage.[20]

In this paper, we reported the characteristics of Ag and Li-doped ZnO nanostructures prepared by hydrothermal method at low temperature on metallic substrates previously covered with ZnO seed layer deposited by spin coating sol-gel method. The obtained nanostructures were covered with a protective PVDF layer with the aim to provide flexibility, robustness, and mechanical resistance to deformation over time and were tested for possible piezoelectric applications.

RESULT AND DISCUSSION

Morphological investigations (AFM and SEM)

To better understand the influence of the experimental parameters on the piezo active properties, the prepared materials were characterized and analyzed in different stages of their realization.

Figure 1a shows 2D topographic AFM images of the 3-layer ZnO (SG) film deposited on a Pt/Ti/SiO_2/Si substrate. From the 2D image scanned at the scale of (8×8) μm^2, it can be seen that the deposition is continuous, uniform and smooth (roughness of a few nm), but shows random small cracks defects, most likely appeared during the heat treatment (probably due to the difference between the expansion coefficient of the substrate and of the deposited film). Scanning an area of (1×1) μm^2 (showed below the corresponding (8×8) μm^2 image) highlights the morphology of the deposited ZnO sol-gel layer, which consists of quasi-spherical uniform particles with a diameter of tens of nm. In certain areas the specific porosity induced by the deposition method is recongnizable.

Figure 1b shows similar AFM images for the 3-layer ZnO (SG) film deposited on Ti substrate. The obvious differences induced by the Ti substrate, observable from the 2D image recorded at the scale of (8×8) μm^2, consist in the presence of some level differences that seem to have the appearance of trenches (probably induced by the specific undulations of the Ti foil used for deposition). From the detailed image at the scale of (1×1) μm^2, it can be seen that the ZnO film completely covers the substrate, being uniform and continuous, with a morphology similar to that observed in the case of the Pt/Ti/SiO_2/Si substrate.

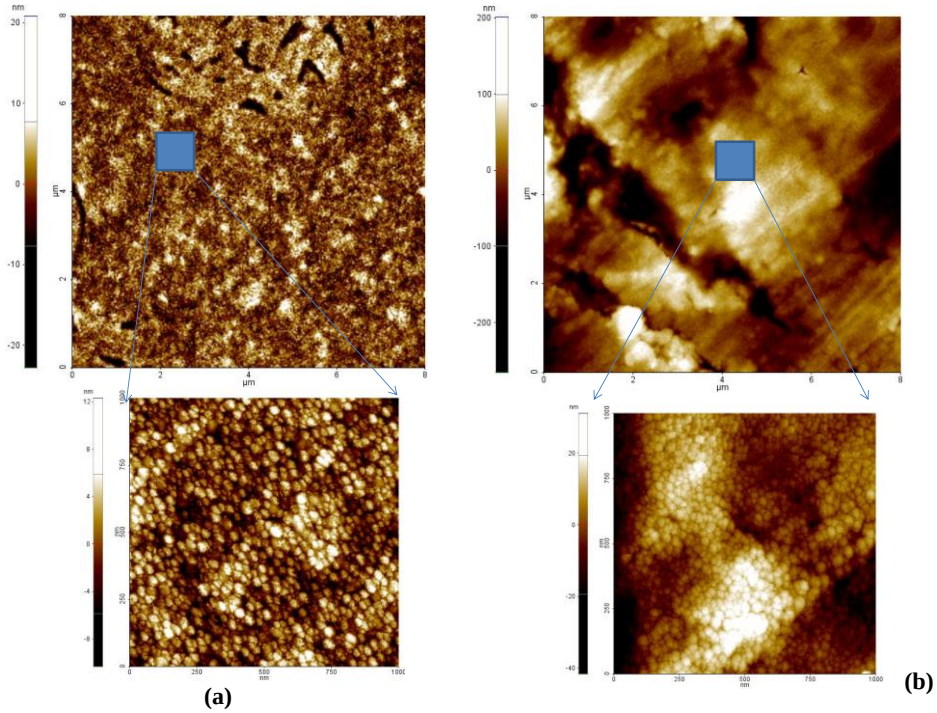

(a) **(b)**

Fig. 1 – 2D topographic AFM images recorded at (8×8)μm^2 (top images) and (1×1)μm^2 (bottom images) of 3-layer ZnO (SG) film deposited on Pt/Ti/SiO_2/Si (a), respectively on Ti (b).

Figure 2a shows a 2D AFM image (enhanced color), recorded at the scale of (8×8) μm^2, together with a characteristic line-scan (horizontal direction) for the Ag-doped ZnO sample, grown by the HT method, on a layer of ZnO-SG, previously deposited on the Pt/Ti/SiO_2/Si substrate. Doping with Ag creates a strong non-uniformity effect, visible through the formation of massive structures, probably arising from the superposition of some bunches of ZnO sticks/rods. The height of these structures is of hundreds of nm, as suggested by the profile line shown in Fig. 2b.

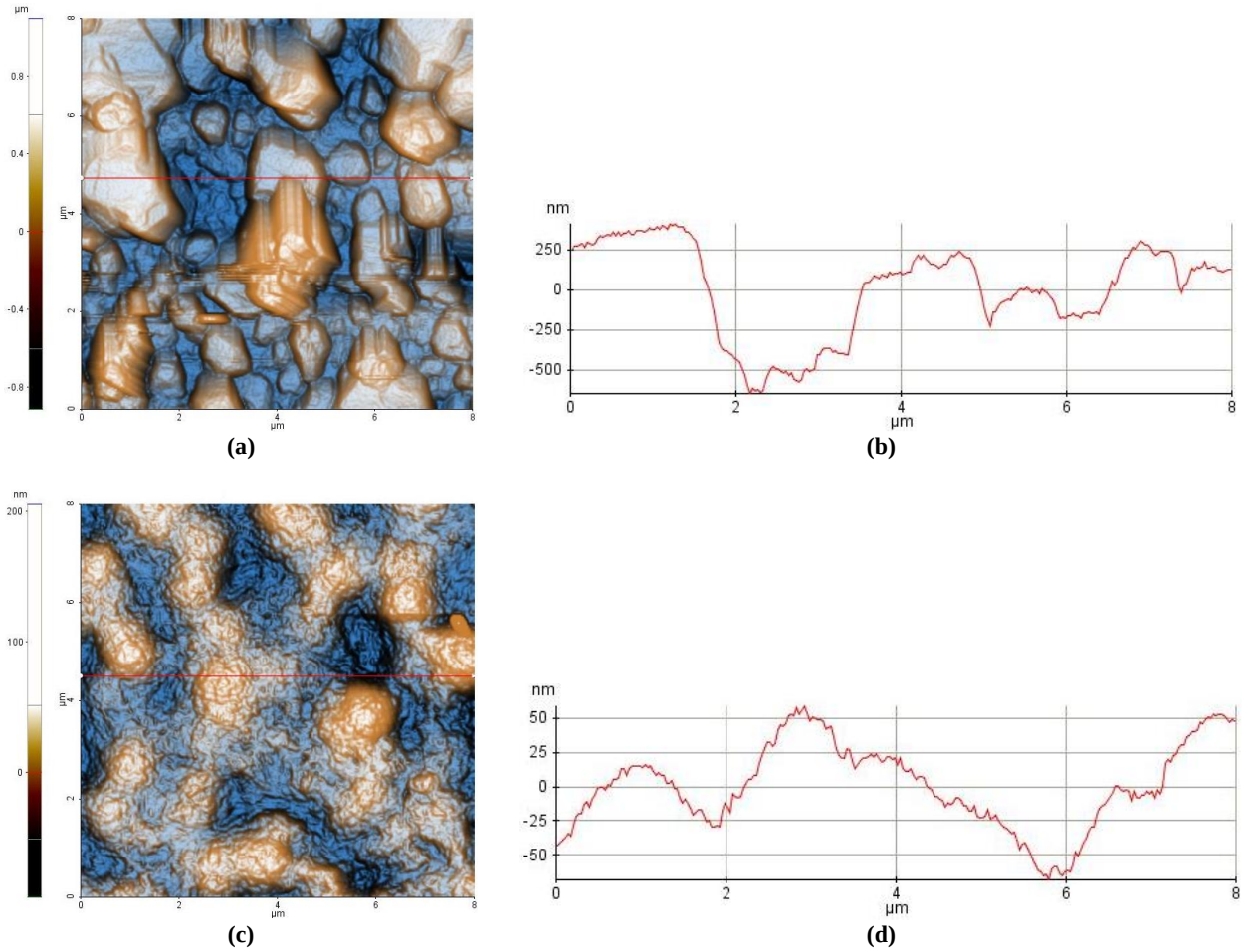

Fig. 2 – 2D AFM (a) together with a line-scan (b) for Ag(HT)-doped ZnO sample deposited on Pt/Ti/SiO_2/Si; 2D AFM image (c) and a line-scan (d) for the PVDF/Ag-doped ZnO sample deposited on Pt/Ti/SiO_2/Si.

Subsequent coating of the Ag(HT)-doped ZnO sample with a layer of PVDV (Fig. 2b) diminishes the morphological inhomogeneities and the corrugation of the Ag-doped ZnO (HT) film deposited on Pt/Ti/SiO_2/Si, leading to a uniform surface with hill-valley structures, whose level difference is about 100 nm (from –50 to +50 nm,) as suggested by the profile line presented in Fig. 2d.

2D AFM image and the line scan (b) of the Ag(HT)-doped ZnO sample deposited on Ti (Fig. 3) also shows the formation of massive structures, suggesting that the dopant favors this rough morphology regardless of the rigid (Pt/Ti/SiO_2/Si) or elastic (Ti) nature of the substrate. These Ag-doped ZnO structures have a slightly higher height in the case of Ti compared to Pt/Ti/SiO_2/Si, as observed from the 2D AFM images and the corresponding profile lines.

The PVDF coating of the Ag-doped ZnO sample deposited on Ti is highlighted in the 2D AFM (c) and the corresponding line-scan (d). In this case, the PVDF layer is influenced by the massive structures of ZnO doped with Ag, but also by the specific unevenness of the Ti foil, resulting in a less uniform coverage with a more pronounced corrugation, of about 400 nm (from –200 nm to + 200 nm), as suggested by the profile line shown in Fig. 3d.

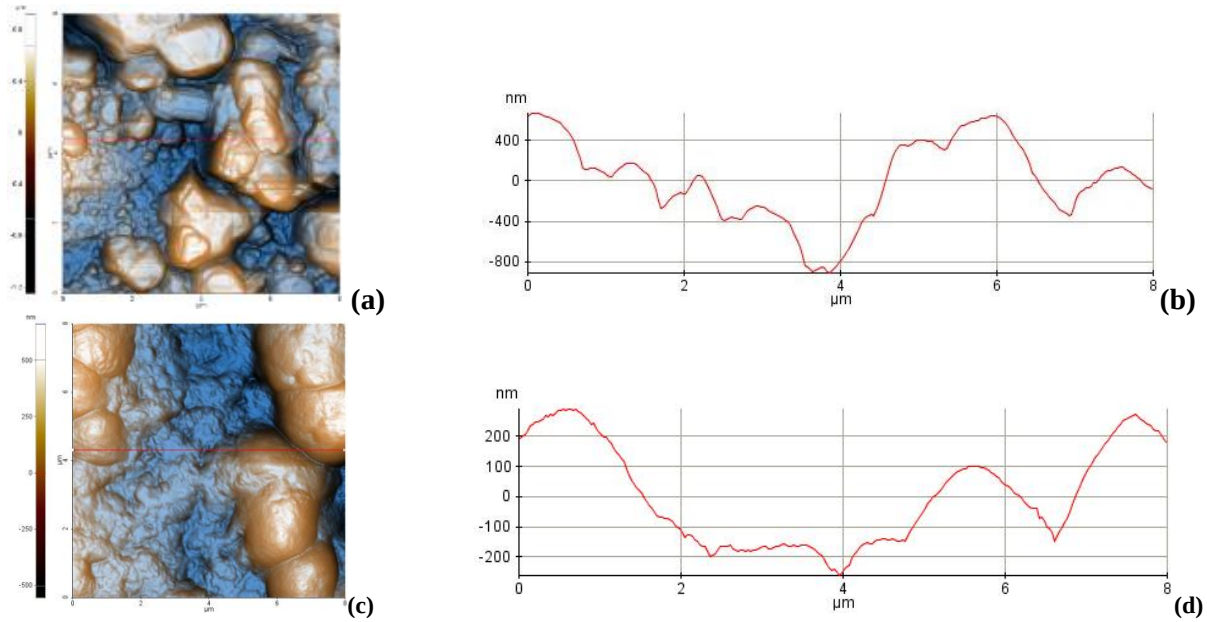

Fig. 3 – 2D AFM image (a) and a line scan (b) for the Ag (HT) doped ZnO sample deposited on Ti; AFM images (c) and a line scan (d) for PVDF/Ag-doped ZnO sample deposited on Ti.

Figure 4a shows the 2D AFM image ((8×8) µm^2 scale) of the Li-doped ZnO coating obtained by the hydrothermal (HT) method of a ZnO sol gel (SG) layer previously deposited on the Pt/Ti/SiO_2/Si substrate (shown in Fig. 1a). It can be seen from Figure 4 that the HT growth of Li-doped ZnO leads to the formation of a continuous and uniform film, consisting in ZnO rods. The 2D AFM image together with the corresponding line-scan from Fig. 4b suggest the formation of a rods-like morphology. This is a confirmation of the preferential nucleation tendency on the (002) direction of ZnO (columnar growth), as consistently observed for ZnO prepared by the hydrothermal method. The ZnO rods are about several hundreds of nm in length as evidenced by the scale of the 2D AFM image and the line-scan (Figs. 4a and 4b).

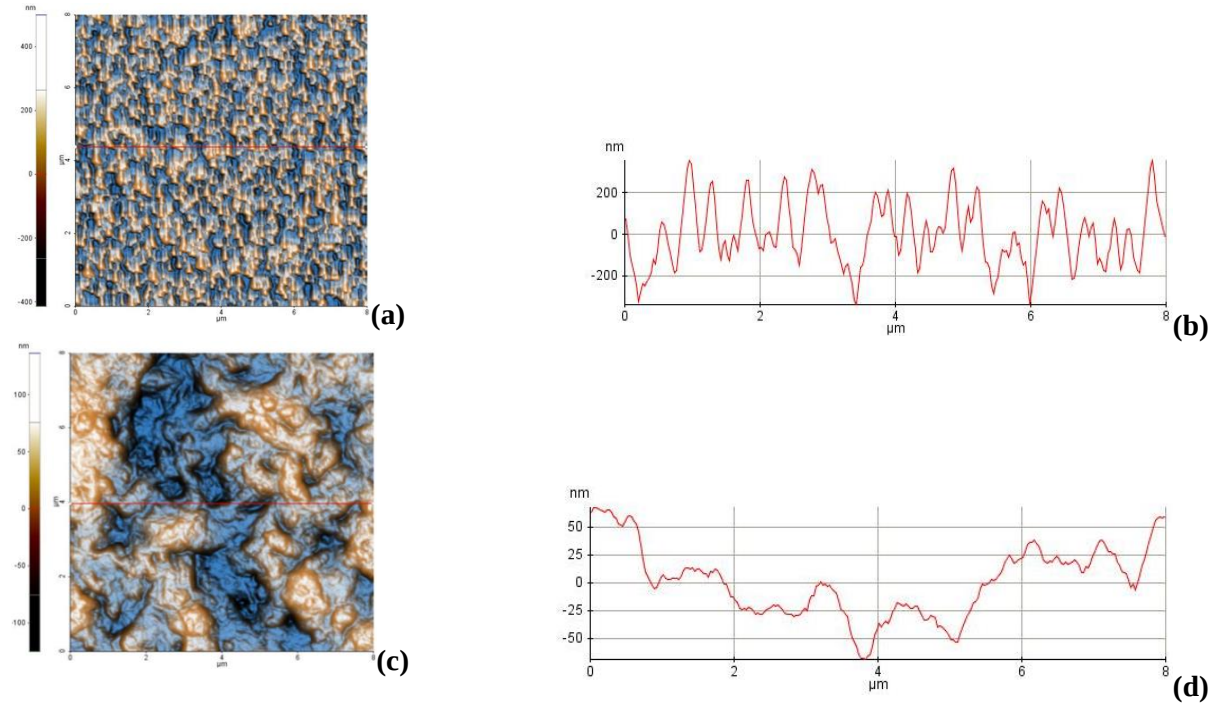

Fig. 4 – 2D AFM image (a) and a line scan (b) for the for the Li-doped ZnO (HT) sample deposited on Pt/Ti/SiO_2/Si; 2D AFM image (c) and a line scan (d) for PVDF/Li-doped ZnO sample deposited on Pt/Ti/SiO_2/Si.

The subsequent deposition of a PVDF layer over the HT/SG film is imaged in Fig. 4c, which shows the 2D AFM image for the PVDF/Li-doped ZnO sample deposited on a $Pt/Ti/SiO_2/Si$ substrate, recorded at the scale of (8×8) μm^2. It can be seen that the PVDF film completely covers the ZnO rods structure, that is, it fulfills its purpose of improving both the elasticity and the piezoelectric behavior of the ZnO-based HT structure. From the profile line shown in Fig. 4d, it can be seen that the level difference of the PVDF film is about 100 nm in the vertical z-axis (from –50 to + 50 nm).

Figure 5a shows the 2D AFM image of the Li-doped ZnO sample (HT deposition) deposited on a Ti substrate, *i.e.* it is compositionally similar to Fig. 4a, the difference being only given by the substrate. The formation of a film composed of ZnO rods can be also observed in this case, with a film (rods) height of several hundred of nm, as suggested by the the profile line shown next to the 2D image (Fig. 5b).

The coating of the ZnO-HT sample (Fig. 5a) with a layer of PVDF is highlighted in the 2D AFM image shown in Fig. 5c (PVDF/Li-doped ZnO sample/Ti substrate). The PVDF layer is somewhat more uniform and smoother in the case of the PVDF/Li-doped ZnO-HT/ZnO SG sample grown on a Ti substrate in comparison with the same structure deposited on a $Pt/Ti/SiO_2/Si$ substrate. The difference in height (vertical direction) of the PVDF coating is about 80 nm (from –40 to +40 nm) as suggested by the profile line exemplified in Fig. 5d.

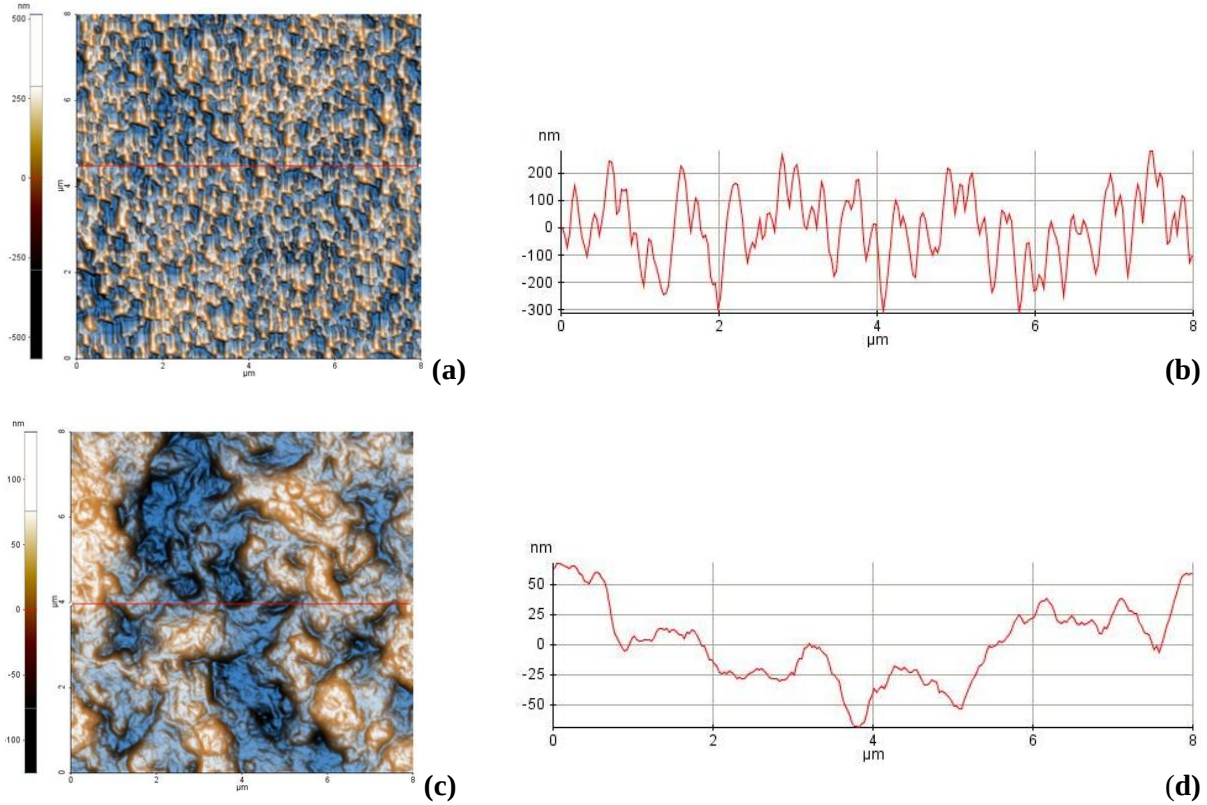

Fig. 5 – 2D AFM image (a) and a line scan (b) for the for the Li (HT) doped ZnO sample deposited on Ti; 2D AFM images (c) and a line scan (d) for PVDF/Li-doped ZnO sample deposited on Ti.

From the micrograph shown in Fig. 6a, the layer of ZnO (SG) deposited on a $Pt/Ti/SiO_2/Si$ substrate can be observed. The morphology of the sol-gel deposited ZnO layer consists of a continuous coating of nanosized particles. Figure 6b shows the formation of a compact layer obtained by growing Ag-doped ZnO by the HT method. The HT-grown layer seems to be the result of the coalescence of vertically growing stick-like structures, as the one marked by an arrow in Fig. 6b, with diameters in the tens of nm, similar to the sizes of the nucleating particles in the SG grown seed layer. The grow of a continuous coating result in a clear inhomogeneity in particle sizes, with particle diameters of hundreds of nms.

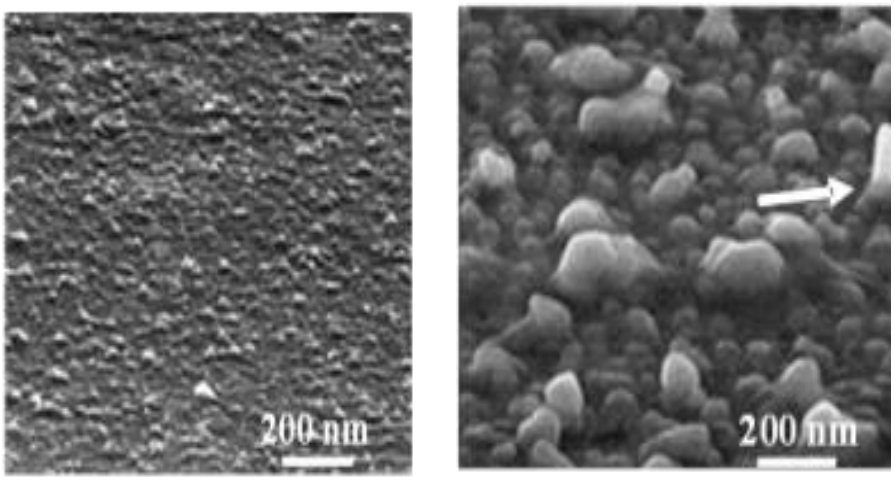

(a) (b)

Fig. 6 – SEM images for ZnO seed layer (a) and the Ag-doped ZnO sample deposited on Pt/Ti/SiO_2/Si substrate (b).

Figure 7 shows the surface morphology of Li-doped ZnO nanowires grown on a sol-gel deposited nucleation layer on Pt/Ti/SiO_2/Si (Fig. 7a) and Ti (Fig. 7b) substrates. After calcination of the substrate with the deposited nucleation layer, in both substrates were obtained vertical nanowires with a uniform c-axis orientation and a high density.

These results demonstrate that the nucleation layer deposited on the substrate has a suitable thickness and particle size to act effectively as a nucleation layer for the grow of a high density layer of homogeneous ZnO nanowires with strong vertical alignment. The ZnO nanowires have similar tip diameter and length, of ~ 60 nm and 1 micron, respectively.

Piezoelectric properties

The assembled devices were measured using the Berlincourt method, under a compressive force of 10 N and a dynamic force of 0.05 N over a frequency range of 35–110 Hz, and they were proved to exhibit piezoelectric properties. In Fig. 8, the measurement results of the direct piezoelectric coefficient d_{33} are graphically represented.

It is observed that the experimental values of the direct piezoelectric coefficient d_{33} increase after polarization, being situated in the range of 0.5 to 2.7 pC/N. Comparing the piezoelectric measurements for the samples deposited on the Pt/Ti/SiO_2/Si substrate (Fig. 9), although the overall values are close for both dopants, it is noticed that the best result was obtained for the PVDF/ZnO sample doped with Ag.

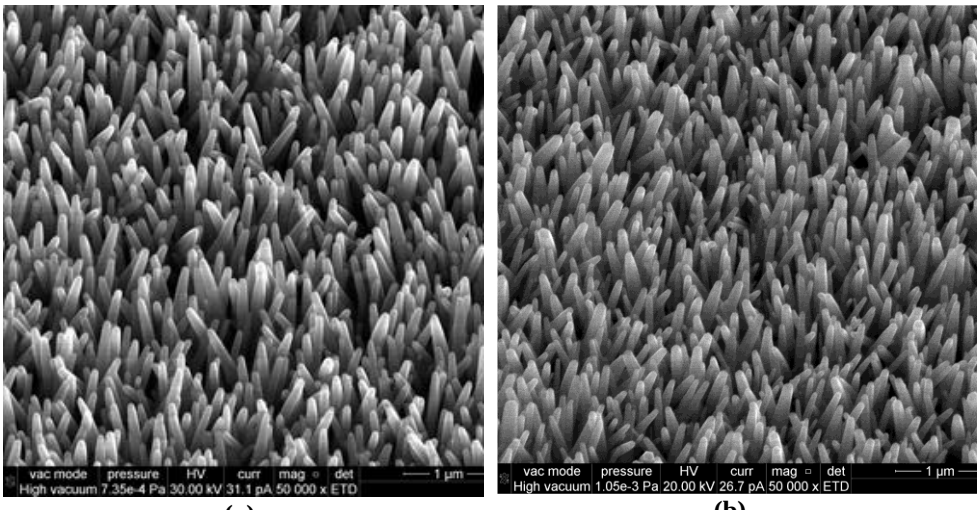

(a) **(b)**

Fig. 7 – SEM images for the ZnO samples doped with Li deposited on Pt/Ti/SiO_2/Si (a) and Ti (b) substrate.

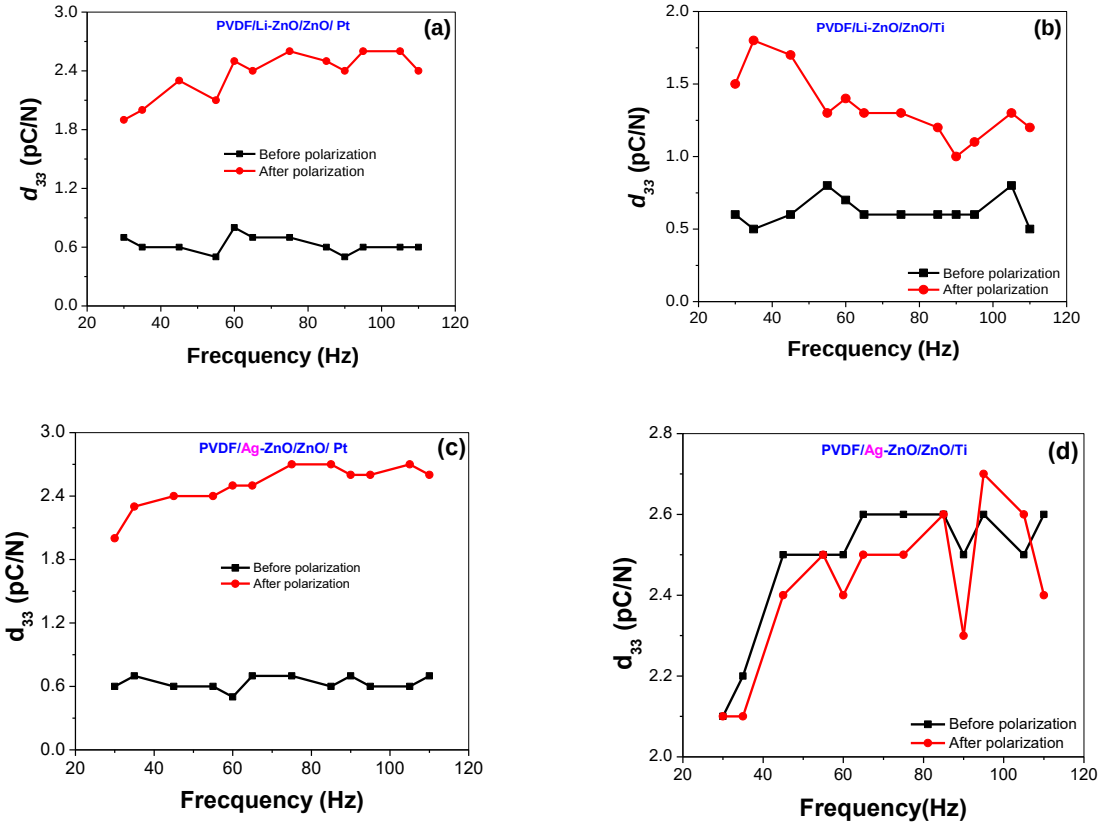

Fig. 8 − Frequency dependence of the piezoelectric coefficient d_{33} for PVDF/ZnO doped with Li (a, b) and Ag (c, d) deposited on Pt/Ti/SiO_2/Si or Ti.

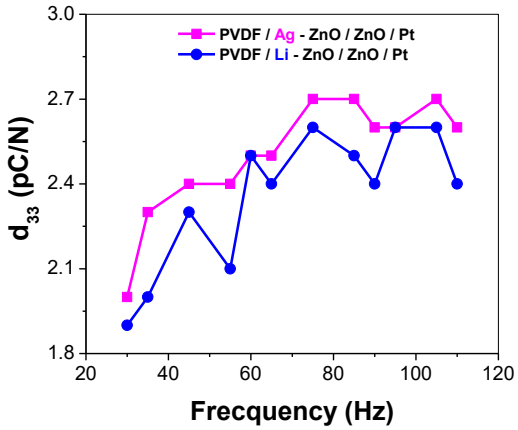

Fig. 9 − Comparative graph of the frequency dependence of the piezoelectric coefficient d_{33} for PVDF/Ag and Li-doped ZnO deposited on Pt/Ti/SiO_2/Si.

EXPERIMENTAL

The metallic substrates chosen for the realization of these models were Pt/Ti/SiO_2/Si and the Ti foil (99% purity), each having the size of 1.5×1.5 cm^2. A ZnO seed layer was grown from a precursor solution prepared by following the steps as reported in Ref. [17]. For the hydrothermal syntheses, the following reagents (Merck, Germany) were used without further purification: $Zn(NO_3)_2{\times}6H_2O$, hexamethylenetetramine ($C_6H_{12}N_4$) (HMTA), silver nitrate ($AgNO_3$), lithium nitrate ($LiNO_3$) (all of 99% purity) and deionized water. Four solutions of 100 mL each were prepared for both substrates, by dissolving the precursor salts of zinc, silver, and lithium. The concentration of the solutions was set at 30 mM and the molar ratio of Ag/Zn and Li/Zn was 1:1. After their complete dissolution, under continuous magnetic stirring, HMTA was added. The metal substrates with ZnO films deposited as nucleation layers were inserted into vessels containing the precursor solution by dipping face down and fixed with Kapton tape. The coated vessels were placed in a preheated oven and maintained at 90 °C

for 10 h. At the end of the reaction, the samples were removed from the solution, washed with distilled water and left to dry overnight. The next day they were thermally treated at 500 ºC for 1 h, with a heating rate of 5 ºC/min.

Assembly of piezoelectric structures

The structures of ZnO nanostructures doped with Ag and Li deposited on Pt/Ti/SiO_2/Si or Ti made in the first two steps were assembled in polymeric matrices from polyvinylidene fluoride solution, [$(C_2H_2F_2)_n$ -], M_w = 534000 (PVDF) (Fig. 10). The following reagents were used for the synthesis: polyvinylidene fluoride (PVDF) (Sigma, M_w = 534000) and N,N-dimethylformamide [C_3H_7NO], (DMF) (Sigma, 99% purity). All Sigma Aldrich reagents were used without further purification. The polymer solution was prepared by dissolving 500 mg of PVDF in 5 mL of DMF, on a hotplate with continuous magnetic stirring, at 75 ºC, until the complete dissolution of the polymer (approximately 3 h). A low viscosity, semi-transparent solution was obtained. The assembly of the piezoelectric structure was done by depositing 15 layers of PVDF by spin coating over the doped ZnO nanowire matrices. The deposition speed was 500 rpm for 10 seconds and 3000 rpm for 30 seconds. The solution was kept on the hotplate at 50 ºC with continuous magnetic stirring and deposited at this temperature on all samples. 15 layers of polymer were deposited as follows: three consecutive depositions, then drying for 3 minutes at 140 ºC on a hot plate, followed by deposition of the second polymer layers, with drying after every three depositions. At the end of the 15 layers deposition, all the samples were dried at 140 ºC for 2 h, on a heated plate. After drying the polymer layer, a thin layer of Ag paste was deposited on top of the samples, forming the upper electrode of the piezoelectric structure. The Ag layers were dried at 110 ºC for several hours on a hot plate. The samples were polarized to induce the formation of the β phase in PVDF.

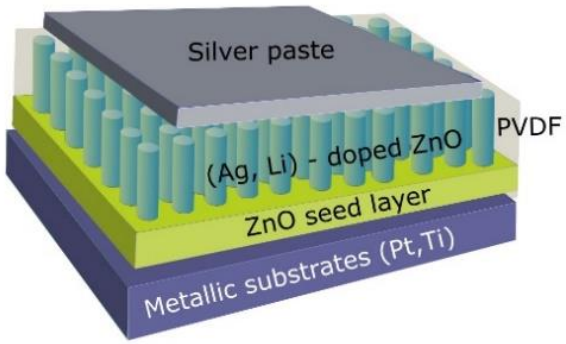

Fig. 10 − Schematic representation of PVDF/Ag and Li-doped ZnO/metallic substrates.

Characterization methods

The morphology was investigated by atomic force microscopy (AFM) and scanning electron microscopy (SEM). AFM measurements were made in non-contact mode using a XE-100 microscope (Park Systems). All AFM images were scanned with sharp tips (NCLR, Nanosensors™) having a radius of curvature < 10 nm, 225 µm mean length, 38 µm mean width, ~48 N/m force constant, and 190 kHz resonance frequency. The recorded AFM images were processed with XEI program (v 1.8.0 – Park Systems). SEM morphology was obtained in top view scanning electron microscopy (SEM) images, using a FEI Quanta 3D microscope operating at 5 kV. The piezoelectric properties of the samples were investigated by measuring the d_{33} (pC/N) piezoelectric coefficients using a Berlincourt type piezometer, PM300 (Piezotest, London, UK).

CONCLUSIONS

In this study, through an easily accessible method, Ag and Li – doped ZnO nanostructures grown on Pt/Ti/SiO_2/Si and Ti foil substrates were synthesized by both the sol-gel method and hydrothermal synthesis at low temperature and further coated with PVDF. The piezoelectric properties of the obtained materials were investigated by measuring the direct piezoelectric coefficient d_{33}. The results showed that the controllable parameters of the chemical synthesis process led to the successful obtaining of nanostructures grown on metallic substrates and their influence on the piezoelectric performance was studied. A slight increase of the piezoelectric response was obtained for the samples doped with Ag, in comparison with those doped with Li, after polarization.

Acknowledgments. The paper was carried out within the research program "Science of Surfaces and Thin Layers" of the "Ilie Murgulescu" Institute of Physical Chemistry and the Romanian Government that allowed for the acquisition of the research infrastructure under POS-CCE O 2.2.1 project INFRANANOCHEM—No. 19/01.03.2009 are gratefully acknowledged.

REFERENCES

1. A. K. Mishra, V.S. J. K. Priya, K. Pradeep, J. S. Vaishnav and G. Kabhilesh, *Materials Today: Proceedings*, **2022**, *62*, 2064–2069.
2. S. D. Mahapatra, P. C. Mohapatra, A. I. Aria, G. Christie, Y. K. Mishra, S. Hofmann and V. K. Thakur, *Adv. Sci.*, **2021**, *8*, 2100864.
3. G. D'Ambrogio, O. Zahhaf, M.-Q. Le, M. Bordet, P. Lermusiaux, N. D. Schiava, R. Liang, P.-J. Cottinet and J-F. Capsal, *Materials & Design*, **2022**, *223*, 111195.
4. M. Sol-Sanchez ´, J.M. Castillo-Mingorance, F. Moreno-Navarro, T. Mattinzioli and M.C. Rubio-Gamez, *Construction and Building Materials*, **2021**, *301*, 124324.
5. F. Ram, J. Garemark, Y. Li and L. Berglund, *Composites Part A*, **2022**, *160*, 107057.
6. A. Ichangi, K. Lê, A. Queraltó, M. Grosch, R. Weißing, F. Ünlü, A. K. Chijioke, A. Verma, T. Fischer, R. Surmenev and Sanjay Mathur, *Adv. Eng. Mater*., **2022**, *24*, 2101394.
7. S. Azimi, A. Golabchi, A. Nekookar, S. Rabbani, M. H. Amiri, K. Asadi and M. M.Abolhasani, *Nano Energy*, **2021**, *83*, 105781.
8. M. Rastgar, J. Fleck, R. Graessner, A. Taghipourand Mohtada Sadrzadeh, *Journal of Membrane Science*, **2022**, *660*, 120819.
9. A. Veved, G. W. Ejuh and N. Djongyang, *Energy Report*, **2022**, *8*, 12853–12870.

10. A. Yusuf, J. Sanchez del Río, X. Ao, I. A. Olaizola and D.-Y. Wang, *Nano Energy*, **2022**, *103*, 107790.
11. M. Chelu, H. Stroescu, J. Calderon Moreno, M. Anastasescu, S. Preda, M. Gartner, C. Moldovan, M. Gheorghe, *Proceedings of the International Conductor Conference-CAS*, **2019**, 315-318.
12. C. L. Cramer, E. Ionescu, M. Graczyk-Zajac, A. T. Nelson, Y. Katoh, J. J. Haslam, L. Wondraczek, T. G. Aguirre, S. LeBlanc, H. Wang, M. Masoudi, E. Tegelerj, R. Riedel, P. Colombo and M. Minary-Jolandan, *Journal of the European Ceramic Society*, **2022,** *42*, 3049–3088.
13. S. M. S. Rana, M. T. Rahman, M. Salauddin, P. Maharjan, T. Bhatta, Hyunok Cho and J. Y. Park, *Nano Energy*, **2020**, *76*, 105025.
14. N. Afsarimanesh, A. Nag, Md. Eshrat e Alahi, S. Sarkar, S. Mukhopadhyay, G. S. Sabet, M. E. Altinsoy, *Sensors and Actuators: A. Physical*, **2022**, *344*, 113743.
15. M. Chelu, J. Calderon Moreno, I. Atkinson, J. Pandele Cusu, A. Rusu, V. Bratan, L. Aricov, M. Anastasescu, A.-M. Seciu-Grama, A. M. Musuc, *International Journal of Biological Macromolecules*, **2022**, *21*, 410–424.
16. H. Sun, S.-J. Park, *Journal of Environmental Sciences*, **2022**, *118*, 57–66.
17. M. Chelu, H. Stroescu, M. Anastasescu, J. M. Calderon-Moreno, S. Preda, M. Stoica, Z. Fogarassy, P. Petrik, M. Gheorghe, C. Parvulescu, C. Brasoveanu, A. Dinescu, C. Moldovan, M. Gartner, *Applied Surface Science*, **2020**, *529*,147135.
18. A. Ichangia, K. Lê, A. Queralto, M. Grosch, R. Weissing, F.Ünlü, A. K. Chijioke, A. Verma, Thomas Fischer, R. Surmenev and Sanjay Mathur, *Adv. Eng. Mater*., **2022**, *24*, 2101394.
19. M. Chelu, P. Chesler, M. Anastasescu, C. Hornoiu, D. Mitrea, I. Atkinson, C. Brasoveanu, C. Moldovan, G. Craciun, M. Gheorghe and M. Gartner, *J. Mater. Sci.: Mater. Electron.*, **2022**, *33*, 19998–20011.
20. L. Ruan, X. Yao, Y. Chang, L. Zhou, G. Qin and X. Zhang, *Polymers*, **2018**, *10*, 228.